



Alterations in brain iron deposition with progression of late-life depression measured by magnetic resonance imaging (MRI)-based quantitative susceptibility mapping

Fang Wang^{1#^}, Ming Zhang^{2#}, Yan Li^{3#}, Yufei Li², Hengfen Gong⁴, Jun Li⁵, Yuyao Zhang⁵, Chencheng Zhang¹, Fuhua Yan³, Bomin Sun¹, Naying He³, Hongjiang Wei^{2,6}

¹Department of Neurosurgery, Center for Functional Neurosurgery, Ruijin Hospital, Shanghai Jiao Tong University School of Medicine, Shanghai, China; ²School of Biomedical Engineering, Shanghai Jiao Tong University, Shanghai, China; ³Department of Radiology, Ruijin Hospital, Shanghai Jiao Tong University School of Medicine, Shanghai, China; ⁴Department of Psychiatry, Shanghai Pudong New Area Mental Health Center, Tongji University School of Medicine, Shanghai, China; ⁵School of Information Science and Technology, ShanghaiTech University, Shanghai, China; ⁶Institute of Medical Robotics, Shanghai Jiao Tong University, Shanghai, China

Contributions: (I) Conception and design: H Wei, B Sun, N He, F Wang, M Zhang, Y Li; (II) Administrative support: H Wei, B Sun; (III) Provision of study materials or patients: H Gong; (IV) Collection and assembly of data: Y Li, N He, F Yan, C Zhang; (V) Data analysis and interpretation: M Zhang, F Wang, YF Li, J Li, H Wei, Y Zhang; (VI) Manuscript writing: All authors; (VII) Final approval of manuscript: All authors.

[#]These authors contributed equally to this work.

Correspondence to: Hongjiang Wei. School of Biomedical Engineering, Shanghai Jiao Tong University, Shanghai 200030, China. Email: hongjiang.wei@sjtu.edu.cn; Naying He. Department of Radiology, Ruijin Hospital, Shanghai Jiao Tong University School of Medicine, Shanghai 200025, China; Email: i@nayinghe.com; Bomin Sun. Department of Neurosurgery, Center for Functional Neurosurgery, Ruijin Hospital, Shanghai Jiao Tong University School of Medicine, Shanghai 200025, China. Email: sbm11224@rjh.com.cn.

Background: Previous studies have revealed abnormality of iron deposition in the brain of patients with depression. The progression of iron deposition associated with depression remains to be elucidated.

Methods: This is a longitudinal study. We explored brain iron deposition with disease progression in 20 patients older than 55 years with depression and on antidepressants, using magnetic resonance imaging (MRI)-based quantitative susceptibility mapping (QSM). Magnetic susceptibility values of the whole brain were compared between baseline and approximately one-year follow-up scans using permutation testing. Furthermore, we examined the relationship of changes between the susceptibility values and disease improvement using Spearman's partial correlation analysis, controlling for age, gender, and the visit interval.

Results: Compared to the initial scan, increased magnetic susceptibility values were found in the medial prefrontal cortex (mPFC), dorsal anterior cingulate cortex (dACC), occipital areas, habenula, brainstem, and cerebellum ($P < 0.05$, corrected). The susceptibility values decreased in the dorsal part of the mPFC, middle and posterior cingulate cortex (MCC and PCC), right postcentral gyrus, right inferior parietal lobule, right precuneus, right supramarginal gyrus, left lingual gyrus, left dorsal striatum, and right thalamus ($P < 0.05$, corrected). Notably, the increase in susceptibility values at the mPFC and dACC negatively correlated with the changes in depression scores, as calculated using the Hamilton Depression Scale (HAMD) ($r = -0.613$, $P = 0.009$), and the increase in susceptibility values at the cerebellum and habenula negatively correlated with the changes in cognitive scores, which were calculated using the Mini-Mental State Examination (MMSE) (cerebellum: $r = -0.500$, $P = 0.041$; habenula: $r = -0.588$, $P = 0.013$). Additionally, the decreased susceptibility

[^] ORCID: 0000-0002-8755-9143.

values at the white matter near the mPFC (anterior corona radiata) also correlated with the changes in depression scores ($r=-0.541$, $P=0.025$), and the decreased susceptibility values at the left lingual gyrus correlated with the changes in cognitive scores ($r=-0.613$, $P=0.009$).

Conclusions: Our study identified brain areas where iron deposition changed with the progression of depression while on antidepressants. The linear relationship of changes in the magnetic susceptibility values in the mPFC, dACC, and some subcortical areas with changes in depression symptoms and cognitive functions of patients is highlighted. Our results strengthen the understanding of the alterations of brain iron levels associated with disease progression in patients with late-life depression.

Keywords: Late-life depression; disease progression; iron deposition; magnetic resonance imaging (MRI); quantitative susceptibility mapping (QSM)

Submitted Nov 25, 2021. Accepted for publication Apr 19, 2022.

doi: 10.21037/qims-21-1137

View this article at: <https://dx.doi.org/10.21037/qims-21-1137>

Introduction

Depression is a common mental disorder mainly characterized by low mood, feelings of sadness, or loss of interest in activities that interfere with a person's everyday activities (1). In addition to experiencing emotional burdens, late-life (older than 55 years) (2,3) depressive patients may also show impairment in various cognitive domains, including attention (4), memory (5,6), information processing speed (7,8), and executive functions (6,9). The neuropathological mechanism underlying depression and its effect on cognition have not yet been fully elucidated, but may be highly associated with multiple neurobiological factors, including the reduction of monoamine neurotransmitters, changes in the hypothalamic-pituitary-adrenal axis, peripheral inflammation, and reduced level of neuroplasticity (1).

Previous neuroimaging studies have also indicated that depression is closely associated with brain structural and functional abnormalities in multiple cortical and subcortical areas, including but not limited to the ventral medial prefrontal cortex (vmPFC), anterior cingulate cortex (ACC), thalamus, and amygdala (10-14). Some neuroimaging features have also been proposed as biomarkers for precise diagnosis or an indication of the dynamic progression of depression. For instance, a resting-state functional magnetic resonance imaging (fMRI) study showed that connectivity in the limbic system regions, such as the vmPFC and ACC, could be used to distinguish between patients with major depression and healthy controls with a high level of accuracy (15). Another fMRI study illustrated that reduced gray matter in the hippocampus was linked to a depressed

state, which may be a potential biomarker of the depressive episode (16).

Iron level, particularly iron deposition in the brain, affects myelination, metabolism, and neurotransmitter levels, and abnormal iron accumulation has been reported in many neurodegenerative diseases (17). Previous research has shown that excessive iron content gives rise to several neurodegenerative diseases, including Parkinson's disease (PD) and Alzheimer's disease (AD) (18,19). Iron deposition may also serve as a biomarker for the onset and progression of neurodegenerative diseases (20,21). Aside from neurodegenerative diseases, iron dysregulation can cause neuronal degeneration or even cell death and, thus, may also influence emotional behavior (22). A previous study indicated that the iron level in the peripheral blood of patients with depression was correlated with the severity of depressive symptoms (23). However, the relationship between iron accumulation and depression is still contradictory. In some studies, patients with lower levels of serum ferritin had a higher prevalence of depressive symptoms (24), while in other studies, researchers found that higher iron levels were associated with more severe depressive symptoms (25). A brain-imaging study revealed increased iron deposition in the putamen and thalamic nuclei in patients with depression, and this brain iron accumulation pattern was related to the severity of depression (26). Moreover, Zhang *et al.* (27) showed that thalamic iron deposits were positively related to depressive symptoms in older adults. Thus, although evidence has only been observed in a limited number of studies, increased iron deposition in some brain areas may be closely associated

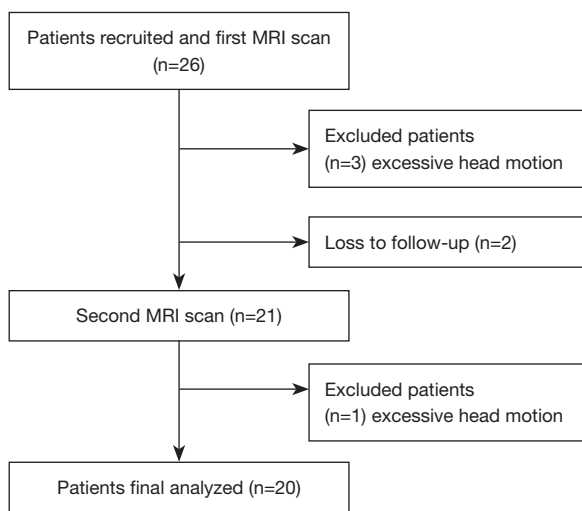


Figure 1 The flow chart of eligible patient inclusion. MRI, magnetic resonance imaging.

with depressive symptoms.

Quantitative susceptibility mapping (QSM) is a novel, non-invasive MRI technique that quantifies the magnetic susceptibility value of brain tissue which has been used to reveal the abnormality of iron deposition in neurodegenerative diseases, such as PD and AD (28,29). In recent years, QSM has also been used to identify brain areas with abnormal iron deposition in psychiatric diseases, including major depressive disorder (MDD) (26,27). However, the alterations in iron deposition associated with the progression of depression have not yet been examined.

In the present study, we imaged the progression of iron deposition in late-life patients for the first time. To do so, we recruited late-life, depressive patients and acquired QSM images from them at baseline and approximately one year later. The brain areas showing altered QSM values between the 2 visits were identified. Furthermore, the relationships between the alterations of the magnetic susceptibility values and the depressive symptoms and cognitive assessment scores in the patients were also examined. We present the following article in accordance with the STROBE reporting checklist (available at <https://qims.amegroups.com/article/view/10.21037/qims-21-1137/rc>).

Methods

Study design

This was a longitudinal study specifically designed to

investigate changes in magnetic susceptibility values of the brain in late-life patients with depression. All participants underwent 2 MRI scans with an interval of approximately 1 year. There was no change in pharmacological treatment between the 2 scans and they took no medication on the day before the scan. Participants were instructed to relax and avoid movement during the scan.

Patient recruitment and criteria

Patients older than 55 years and diagnosed by a psychiatrist at Shanghai Pudong New Area Mental Health Center with depression according to the criteria in the International Classification of Diseases [ICD-10; V. Mental and behavioral disorders/F30-F39 Mood (affective) disorders/F32 Depression episode] (30) were recruited into the study from 2014 to 2016. Patients with a history of severe head trauma, alcohol abuse, claustrophobia, psychiatric diseases other than depression, or metal or electronic implants were excluded. We recruited a total of 26 eligible patients to our study. In all, 4 patients with excessive head motion that prevented proper image assessment (3 in the first scan, 1 in the second scan) were excluded; 2 patients were lost to follow-up. A total of 20 patients were included in the analysis of the study. The flow diagram of patient selection is shown in *Figure 1*. The mean age of the patients was 63.1 ± 6.2 years (range, 55–78 years).

All patients enrolled were treated with selective serotonin reuptake inhibitors (SSRIs) (sertraline, escitalopram, citalopram, or paroxetine) or other antidepressants (venlafaxine, mirtazapine, olanzapine, or trazodone), and about half of the patients (9/20) took more than 1 antidepressant. There was no change in pharmacological treatment between the 2 scans, and all patients took their drugs regularly during the 1-year follow-up with good compliance. During the follow-up period, the only treatment that participants received was their medication.

The study was conducted in accordance with the Declaration of Helsinki (as revised in 2013) and approved by the Ethics Committee of Shanghai Pudong New Area Mental Health Center (No. PDJWLL2014001). All patients were fully informed about the procedures and provided written informed consent.

Clinical evaluation

Demographic and clinical information was collected from the participants. Clinical information mainly included

the duration of depression and details of medication. Psychological and cognitive measurements were performed immediately before the patients were scanned in the magnetic resonance machine. Depressive symptoms were evaluated by an experienced psychiatrist using the Hamilton Depression Scales (HAMD-17 and HAMD-24) (31). In the HAMD-17, total scores were translated as: <8, normal; 8–17, mild depression; 18–24, moderate depression; and >24, severe depression. In the HAMD-24, total scores were interpreted as: <8, normal; 8–20, mild depression; 21–35, moderate depression; and >35, severe depression. Anxiety symptoms were evaluated using the Hamilton Anxiety Scale (HAMA) (32), and the total scores interpreted as: <7, normal; 7–13, mild anxiety; 14–20, moderate anxiety; 21–28, significant anxiety; and >28, severe anxiety. Cognitive functions were assessed via the Montreal Cognitive Assessment (MoCA; total scores interpreted as: ≥ 26 , normal; 18–25, mild cognitive impairment; 10–17, moderate cognitive impairment; and <10, severe cognitive impairment) (33) and the Mini-Mental State Examination (MMSE; total scores interpreted as: ≥ 27 , normal; 21–26, mild cognitive impairment; 10–20, moderate cognitive impairment; and <10, severe cognitive impairment) (34). At 11 to 18 months after the first session, the patients attended the second session, during which they were reevaluated for depression, anxiety, and cognitive functions, and were scanned for a second time.

MRI protocol

The MRI scans were performed at the Ruijin Hospital, Shanghai Jiao Tong University School of Medicine, Shanghai, China. On the day of the scanning, the patients did not take medication. Each patient underwent an MRI scan on the same 3.0-T clinical MRI scanner (Signa HDxt, General Electric Healthcare, Milwaukee, WI, USA) using an 8-channel phased-array head coil during the first and second visits. The patients lay supine with their heads snugly fixed by foam pads. The patients were asked to keep still for as long as possible during scanning. The MRI measurements consisted of a T1-weighted magnetization-prepared rapid acquisition gradient-echo (MP-RAGE) sequence for anatomical structures and a three-dimensional (3D) gradient-recalled echo (GRE) sequence for QSM, both in sagittal view.

The T1-weighted MP-RAGE image was obtained with the following parameters: repetition time (TR) = 5.6 ms; echo time (TE) = 1.7 ms; inversion time = 450 ms; flip angle = 12°; field of view (FOV) = 256 × 256 × 196 mm³; matrix size

= 256 × 256 × 196; voxel resolution = 1 × 1 × 1 mm³; total scan time = 4 minutes 20 seconds. The multi-echo GRE sequence was performed with the following parameters: TR = 59.3 ms; number of echoes = 16; TE1/ΔTE/TE16 = 2.7/2.9/45.8 ms; bandwidth = 62.5 kHz (488.28 Hz/pixel); flip angle = 12°; FOV = 220 × 220 × 136 mm³; matrix size = 256 × 256 × 136; voxel resolution = 0.86 × 0.86 × 1.00 mm³; acceleration factor = 2; and total scan time = 10 minutes 42 seconds.

Reconstruction of QSM images

The pipeline of image processing and data analysis is shown in *Figure 2*. The QSM images were reconstructed from GRE data using the STI Suite v3.0 toolbox in MATLAB R2019b (MathWorks, Natick, MA, USA). The details of QSM processing have been documented in previous studies (35,36). The brain mask was generated based on the magnitude image of the second echo using the Brain Extraction Tool (BET) (37) in Functional Magnetic Resonance Imaging of the Brain (FMRIB) Software Library v6.0 (FSL; Oxford University, UK; <https://fsl.fmrib.ox.ac.uk/fsl/fslwiki/FSL>) package. The 3D phase image was first unwrapped with the Laplacian-based method (38). For background phase removal, the tissue phase was estimated from the unwrapped phase for each echo using a variable-kernel sophisticated harmonic artifact reduction for phase data (V_SHARP) method (39). Lastly, magnetic susceptibility was quantitatively calculated by dipole inversion using a 2-step field-to-source method called streaking artifact reduction for QSM (STAR-QSM) (35). The susceptibility value was not referenced to any specific areas. Instead, the mean susceptibility value of the whole brain was used as a reference. In this study, the signed, rather than the absolute value of magnetic susceptibility, was used for analysis.

Spatial normalization of QSM images

The GRE magnitude used for registration was obtained by summing the squares of the magnitude images among different TEs. The frequency intensity non-uniformities of the MP-RAGE and GRE magnitude images were corrected using the “N4BiasFieldCorrection” function (40) in Advanced Normalization Tools v2.1 (ANTs; <http://stnava.github.io/ANTs/>). The skulls of the MP-RAGE and magnitude images were stripped using BET in FSL. Using all MP-RAGE images, the T1-weighted study-wise template was then created by the “antsMultivariateTemplat

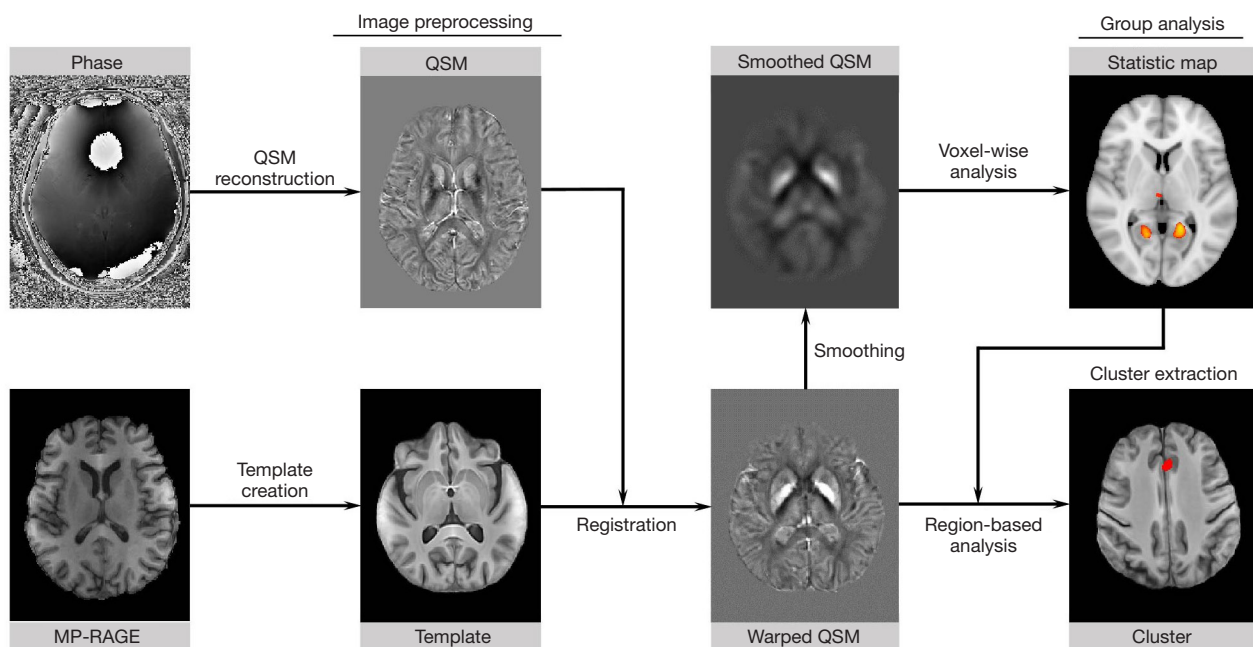


Figure 2 Summarized steps of the pipeline for image preprocessing and group statistical analysis. QSM, quantitative susceptibility mapping; MP-RAGE, magnetization-prepared rapid acquisition with gradient echo.

eConstruction2.sh” script (41,42) in ANTs with an isotropic resolution of 1 mm.

The GRE magnitude image was affinely standardized to its corresponding MP-RAGE image. The individual MP-RAGE image was nonlinearly registered to the study-wise, T1-weighted template. Then, the QSM image, in the same space as the magnitude image, was normalized to the study-wise space using the transformations above with linear interpolation. These registration steps were performed using “antsRegistrationSyN.sh” and “antsApplyTransforms” functions (43) in ANTs. After these procedures, a study-wise QSM template was generated from the average of the warped QSM images.

Whole-brain voxel-wise analysis

The spatially registered QSM images were smoothed with a Gaussian kernel (standard deviation =3 mm) to reduce the errors during registration and enable group comparisons. To determine the progression of iron deposition in depressive patients, a permutation test was performed to identify the brain areas with significant differences between the 2 visits. The whole-brain voxel-wise permutation was conducted using the “randomize” command in FSL with a paired design (44). The age, gender, and time interval

between 2 visits were treated as the nuisance covariates. The permutation time was set as 5,000, and the threshold-free cluster enhancement (TFCE) was used as the test statistic. The reported P value was family-wise error (FWE)-corrected. The statistical significance of whole-brain analysis was defined as FWE-corrected $P < 0.05$. After permutation analysis, the study-wise QSM template and statistical results were warped to the Montreal Neurological Institute (MNI) space (McGill University, Montreal, Canada) for further visualization.

Statistical analysis

The data of patients with excessive head motion or lost to follow-up were excluded. The clusters showing significantly altered magnetic susceptibility values in the voxel-wise analysis were extracted in the study-wise space by applying the “cluster” function in FSL. It should be noted that it was the unsmoothed susceptibility value that was used for the region of interest (ROI) analysis.

The median QSM values were extracted from each cluster for statistical analysis, which was performed using the software SPSS 23.0 (IBM Corp., Armonk, NY, USA). The comparison of the clinical scores between the 2 visits was performed using the paired t -test, and

Table 1 Participant demographic and clinical information

Measure	First visit (n=20)	Second visit (n=20)	P value	95% CI
Gender (male/female)	7/13	7/13	–	–
Age at baseline (years)	63.1 (6.2)	64.3 (6.2)	–	–
Disease duration (years)	9.9 (10.4)	11.2 (10.4)	–	–
Interval between visits (months)	–	15 (2.1)	–	–
Antidepressant medicine		Sertraline (n=2)	–	–
		Escitalopram (n=2)		
		Citalopram (n=4)		
		Paroxetine (n=1)		
		Venlafaxine (n=1)		
		Mirtazapine (n=1)		
		Escitalopram & mirtazapine (n=3)		
		Venlafaxine & mirtazapine (n=2)		
		Escitalopram & trazodone (n=1)		
		Escitalopram & trazodone & olanzapine (n=1)		
		Paroxetine & mirtazapine (n=1)		
		Citalopram & mirtazapine (n=1)		
HAMD-17 scores	16.9 (8.1)	10.9 (8.9)	0.0053	–12.82 to –3.378
HAMD-24 scores	22.5 (11.4)	14.4 (12.0)	0.0019	–9.994 to –2.006
HAMA scores	16.3 (8.6)	8.9 (8.1)	<0.0001	–10.53 to –4.268
MoCA scores	25.2 (3.9)	25.2 (4.0)	0.902	–0.8882 to 0.7882
MMSE scores	28.1 (2.1)	28.2 (1.3)	0.785	–0.6577 to 0.8577

The values of variables are presented in the form of the mean (standard deviation). CI, confidence interval; HAMD, Hamilton Depression Scale; HAMA, Hamilton Anxiety Scale; MoCA, Montreal Cognitive Assessment; MMSE, Mini-Mental State Examination.

$P < 0.05$ was considered significant. Spearman's partial correlation analysis was used to assess the relationship between the alterations in clinical scores (HAMD-17, HAMD-24, HAMA, MMSE, and MoCA) and the QSM changes between 2 visits, controlling for age, gender, and the visit interval. Multiple comparisons were corrected using the Bonferroni correction with a factor of 23 (12 ROIs of increased QSM values and 11 ROIs of decreased QSM values) to reduce the type I error ($P < 0.0022$ was the corrected threshold of $P < 0.05$, by Bonferroni correction).

Results

Demographics and clinical measurements

A total of 26 patients with late-life depression were

recruited, and all of them underwent the first MRI scan. As 3 patients with excessive head motion that prevented proper image assessment were excluded and 2 patients were lost to follow-up, the 21 remaining patients underwent the second MRI scan. We excluded 1 patient due to excessive head motion in the second scan. A total of 20 patients with late-life depression were included in the final analysis. The flow diagram of patient selection is shown in *Figure 1*. The mean follow-up time was 15 ± 2.1 months (range, 11–18 months). The age, gender, mean disease duration, and clinical assessments (HAMD-17, HAMD-24, HAMA, MMSE, and MoCA scores) of the 2 visits of the patients are presented in *Table 1*. The patients received medication of SSRIs (sertraline, escitalopram, citalopram, or paroxetine) or other antidepressants (venlafaxine, mirtazapine, olanzapine, or

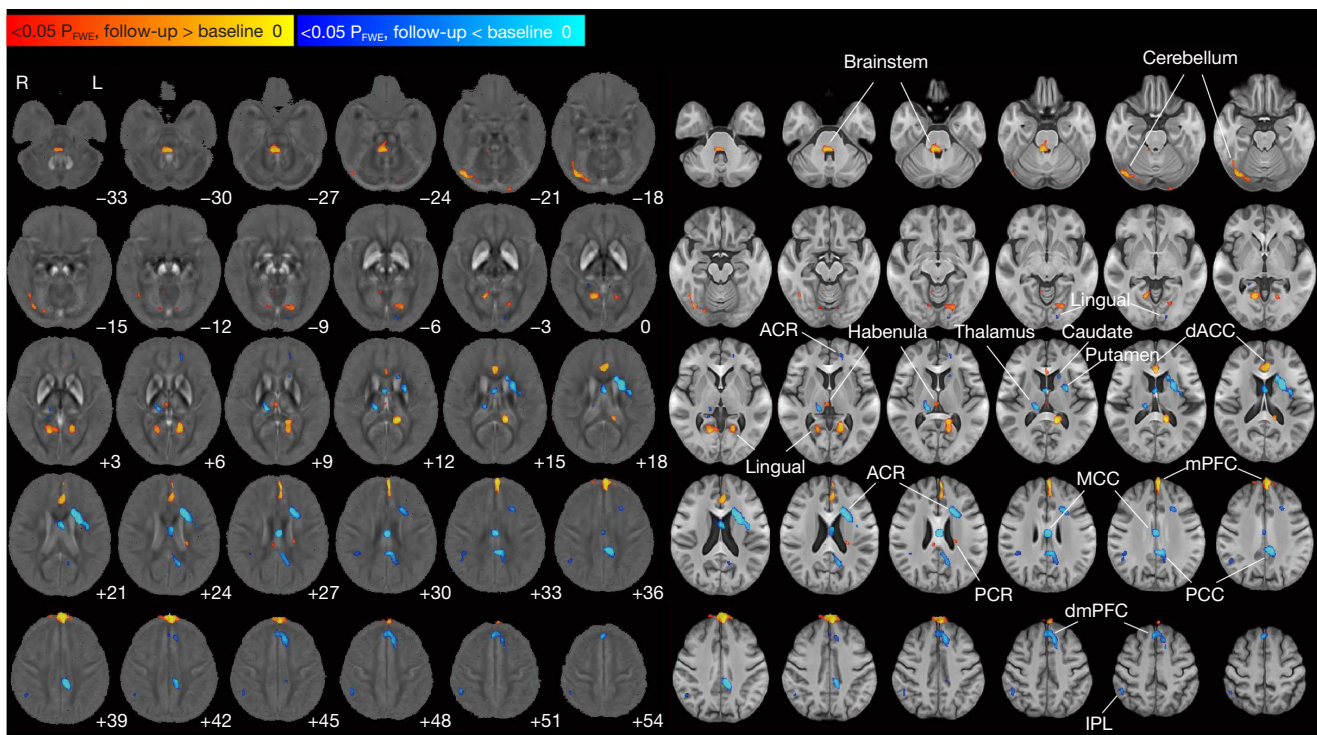


Figure 3 Changes in patient whole-brain susceptibility values after approximately 1 year, overlaid on the QSM template and T1 template in the MNI space by voxel-wise analysis. The red/yellow clusters represent a higher susceptibility value in the follow-up/second visit ($P < 0.05$, FWE-corrected). The blue/light blue clusters represent a lower susceptibility value in the follow-up/second visit ($P < 0.05$, FWE-corrected). The numbers represent the axial coordinates of the slice in millimeters in the MNI coordinate space ($P < 0.05$, FWE-corrected). FWE, family-wise error; ACR, anterior corona radiata; dACC, dorsal anterior cingulate cortex; MCC, middle cingulate cortex; mPFC, medial prefrontal cortex; PCR, posterior corona radiata; PCC, posterior cingulate cortex; dmPFC, dorsal medial prefrontal cortex; IPL, inferior parietal lobule; QSM, quantitative susceptibility mapping; MNI, Montreal Neurological Institute.

trazodone) during the year between the 2 visits. The MoCA and MMSE scores did not show significant changes in the second visit ($P > 0.05$), while the scores on the HAMD-17, HAMD-24, and HAMA, significantly decreased after 1 year, indicating a decrease in the depression and anxiety level ($P < 0.01$, $P < 0.01$, $P < 0.0001$ for HAMD-17, HAMD-24, and HAMA, respectively).

Patient brain areas showing changed susceptibility values after 1 year

The susceptibility values were compared to identify the brain areas associated with the progression of iron deposition in patients with depression on antidepressants. The susceptibility values of the patients between the 2 visits were quantitatively compared, and the brain areas showing a significant alteration in susceptibility values ($P < 0.05$, FWE-corrected)

are shown in *Figure 3* and summarized in *Tables S1,S2*. The susceptibility values showed an increase in the medial prefrontal cortex (mPFC), dorsal anterior cingulate cortex (dACC), occipital areas (the calcarine, lingual, and fusiform gyri), habenula, brainstem, and the cerebellum compared with the values of 1 year before ($P < 0.05$, FWE-corrected; *Figure 4A*). The susceptibility values decreased in the dorsal medial prefrontal cortex (dmPFC; anteriorly close to the supplementary motor area), middle and posterior cingulate cortex (MCC and PCC), right postcentral gyrus, right parietal areas (the inferior parietal, right precuneus, and right supramarginal areas), left lingula, left dorsal striatum (the caudate and putamen), and right thalamus ($P < 0.05$, FWE-corrected; *Figure 4B*). Some white-matter regions also showed alterations. The anterior corona radiata showed a decreased susceptibility value, and the posterior corona radiata showed an increased susceptibility value. The

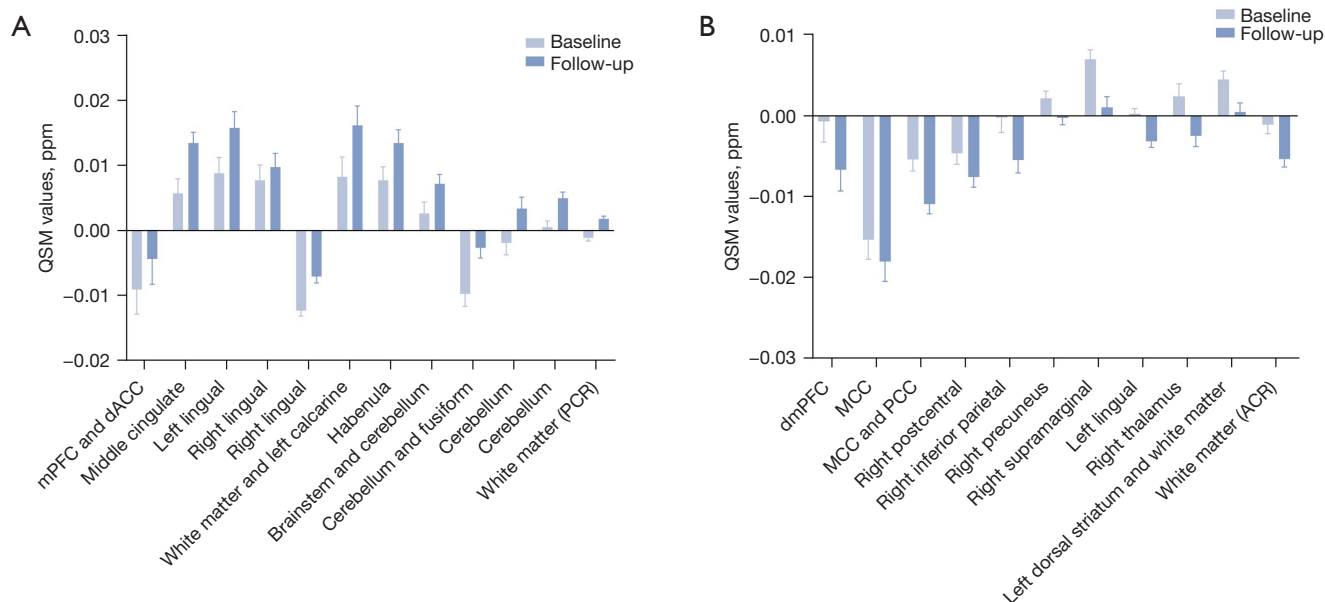


Figure 4 Comparison of magnetic susceptibility values of each cluster between the 2 visits. (A) The increased magnetic susceptibility value in the mPFC, dACC, occipital areas, habenula, brainstem, and the cerebellum compared with that of 1 year previously ($P < 0.05$, FWE-corrected). (B) The decreased susceptibility value in the dmPFC, MCC and PCC, right postcentral, right inferior parietal, right precuneus, right supramarginal, left dorsal striatum, and right thalamus ($P < 0.05$, FWE-corrected). Values represent the mean and SEM. QSM, quantitative susceptibility mapping; ppm, parts per million; mPFC, medial prefrontal cortex; dACC, dorsal anterior cingulate cortex; PCR, posterior corona radiata; dmPFC, dorsal medial prefrontal cortex; ACR, anterior corona radiata; FWE, family-wise error; MCC, middle cingulate cortex; PCC, posterior cingulate cortex; SEM, standard error of the mean.

sagittal projections of the whole-brain susceptibility values changed after approximately 1 year in the patients, which are overlaid on the QSM template and the T1 atlas in the MNI space shown for reference in [Figure S1](#).

Relationship between alterations in susceptibility values and changes in depressive symptoms and cognition

The relationships between the changes in iron deposition and the alterations in depressive symptoms and cognition were further examined by a partial Spearman correlation adjusted for age, gender, and the interval between the 2 visits. The QSM signals were extracted from the areas with changed susceptibility in the second visit. Before the correction for multiple comparisons, we found the increase of QSM value in the mPFC and dACC was negatively correlated with the decrease in the HAMD-17 scores ($r = -0.613$, $P = 0.009$) ([Figure 5A](#)) and HAMD-24 scores ($r = -0.542$, $P = 0.025$) ([Figure 5B](#)), and the increase of the QSM value in the cerebellum and habenula was negatively correlated with the increase in the MMSE scores ($r = -0.500$,

$P = 0.041$; $r = -0.588$, $P = 0.013$, respectively) ([Figure 5C, 5D](#)). Additionally, the decrease in the QSM value in the white matter near the mPFC (at the anterior corona radiata, the cluster peaked at $x = -18$, $y = 44$, $z = 6$ mm in the MNI space) was negatively correlated with the decrease in the HAMD-17 scores ($r = -0.541$, $P = 0.025$) ([Figure 5E](#)) and HAMD-24 scores ($r = -0.500$, $P = 0.041$) ([Figure 5F](#)), and the decrease in the QSM value in the left lingula was negatively correlated with the increase in the MMSE scores ($r = -0.613$, $P = 0.009$) ([Figure 5G](#)). After Bonferroni correction, none of the changes in the QSM values after 1 year were significantly correlated with alterations in depressive symptoms (HAMA, HAMD-17, and HAMD-24 scores; all $P > 0.0022$) or cognition (MMSE and MoCA scores; all $P > 0.0022$) ([Tables S3, S4](#)).

Discussion

Objective biomarkers for the onset and progression of depression are helpful for accurate diagnosis and evaluation and may help to improve the clinical interventions for the disorder. Excessive iron has been shown to contribute to

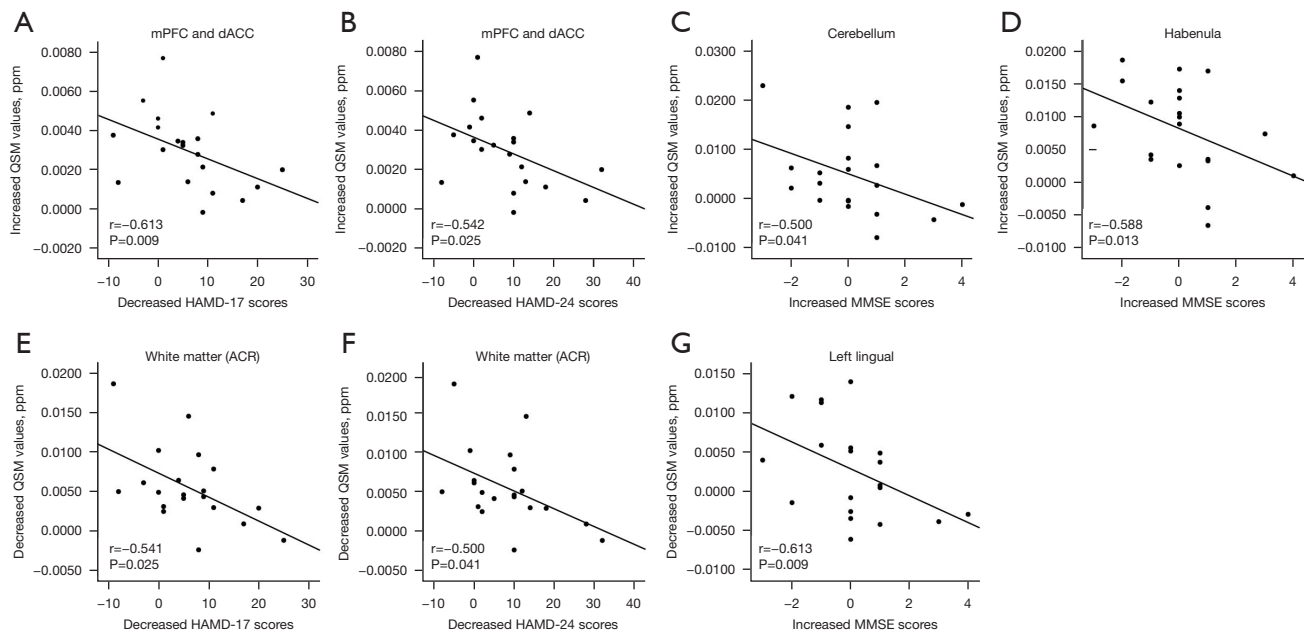


Figure 5 Correlation between the changes in QSM values and the changes in depression and cognitive measurements. (A,B) The correlation between the increased QSM values in the mPFC and dACC and the decreased HAMD-17 scores (A) and the HAMD-24 scores (B). (C,D) The correlation between the increased QSM values in the cerebellum (C), habenula (D), and the increased MMSE scores. (E,F) The correlation between the decreased QSM values in the white matter near the mPFC (anterior corona radiata) and the decreased HAMD-17 scores (E) and the HAMD-24 scores (F). (G) The correlation between the decreased QSM values in the left lingual lobe and the increased MMSE scores. The r and P values are derived from partial Spearman correlation analyses adjusted for age, gender, and the interval between the 2 visits ($P < 0.05$). QSM, quantitative susceptibility mapping; ppm, parts per million; HAMD, Hamilton Depression Scale; mPFC, medial prefrontal cortex; dACC, dorsal anterior cingulate cortex; MMSE, Mini-Mental State Examination; ACR, anterior corona radiata.

some abnormal physiological brain functions, and iron may be a potential biomarker for depression and its progression. Our study used QSM for the first time to identify the brain areas where iron deposition changed as depression progressed in patients with late-life depression. Specifically, the mPFC, dACC, occipital areas, habenula, brainstem, and cerebellum showed increased magnetic susceptibility values. Additionally, the dmPFC, MCC and PCC, parietal and occipital areas, thalamus, and dorsal striatum (caudate and putamen) showed decreased susceptibility values after approximately 1 year of disease progression in patients being treated with antidepressants. Notably, the changed susceptibility values in the mPFC, dACC, and nearby white matter (anterior corona radiata) after 1 year were negatively correlated with the changes in depression scores, and the changed susceptibility values in the cerebellum, habenula, and left lingula after approximately 1 year were negatively correlated with the changes in cognitive scores, although this was not significant after correction for multiple

comparisons.

Abnormal brain iron deposition and depression

While the relationship between abnormal magnetic susceptibility values representing elevated iron deposition and the progression of neurodegenerative diseases has been well established, the relationship between magnetic susceptibility values and the neuropathology of psychiatric diseases remains to be elucidated. To our knowledge, only a few studies have reported the abnormality of brain iron deposition measured by QSM. A brain imaging study revealed increased iron deposition in the putamen and thalamus nucleus of patients with depression, and this brain iron accumulation pattern was related to the severity of depression (26). Moreover, Zhang *et al.* (27) showed that thalamic iron deposits were positively related to depressive symptoms in older adults. Thus, although evidence has only been observed in a limited number of studies, increased iron

deposition in some brain areas may be closely associated with depressive symptoms. However, the alterations in iron deposition associated with the progression of depression remain yet to be examined. The examination of the alterations in susceptibility values associated with depression would help elucidate the dynamic progression of brain iron deposition in this disorder.

Changed susceptibility in the cortical areas during the progression of depression

In the present study, iron accumulation changed both in the cortical areas and subcortical areas in late-life depressive patients. Iron deposition in the mPFC, dACC, and occipital areas was significantly changed. In particular, the increased QSM values of mPFC and dACC were negatively correlated with the alteration in depression scores. As the depressive symptoms improved, the increased QSM values in the mPFC and dACC were decreased. The mPFC and ACC are part of the cortical midline structures (CMS), which serve as the neural underpinnings of self-referential processing in healthy people (45). Dysfunction within the CMS may induce disturbances in emotional behavior, problem-solving, decision-making, and cognitive processing in patients with MDD (46).

Several studies have shown that mPFC is dysregulated and shows an abnormal structure in patients with depression (47). Furthermore, various therapies for the treatment of depression seem to modulate the activity of the PFC or PFC-involved circuit as the antidepressant mechanism (48-50). It has also been reported that iron deposition could affect the functional coherence between cortical and subcortical areas (51). Therefore, increased iron accumulation may contribute to the abnormal neuronal activity of mPFC, change the local processing of input information and output pathological information which affect the functional activities of the brain areas connected to the mPFC, and lead to episodes of depression. Our findings identified the link between the iron deposition in mPFC and depression, further highlighting the affected mPFC (PFC) function with depression.

The MRI and magnetic resonance spectroscopy (MRS) studies also suggest that 1 of the most promising biomarkers in MDD might be the activities in the ACC (52). The alterations of regional homogeneity of the ACC might be associated with depression duration and severity in MDD patients (53). The changed susceptibility value of the dACC in our study further illustrates the role of ACC in depression.

Previous studies have found that the occipital lobe is also involved in depression. The occipital lobe consists of the primary visual cortex and associative visual areas, which mainly participate in perception and visual information processing, as well as in interpreting and drawing conclusions about visual images. A resting-state fMRI study showed that the regional homogeneity of the bilateral occipital lobe decreased in patients with depression (54). Another study found that the activation of the occipital lobe decreased in patients with depression during an emotional picture-processing task (55). These pieces of evidence suggest that the dysfunction of the occipital lobe may be involved in the abnormality of emotional and cognitive functions of depressed patients, which is possibly related to the generation of oxidative reactions and neurotoxicity under elevated iron levels (56), and eventually affects the neural activities in this area.

Our observations of increased iron deposition in the mPFC, dACC, and occipital areas suggest that these cortical midline areas may be adversely affected around the 1-year progression of depression with antidepressant treatment.

Aside from the cortical brain areas showing an increase in susceptibility as depression progressed, cortical areas showing a decrease in susceptibility were also found. The QSM values in the MCC and PCC and the parietal areas (right precuneus, right supramarginal gyrus, and right inferior parietal lobule) decreased in the second scan. Abnormal functional connectivity between the PCC and the brain areas associated with reward processing, salience, and executive functions has been found in MDD patients (57,58), suggesting a critical role of the PCC in the pathological basis of depression. Previous studies have reported that structural and functional abnormalities of the precuneus are associated with depression. In a study, at the resting state, the spontaneous neural activity of the precuneus in MDD patients was impaired (59). In another study, functional connectivity changed in patients with depression among the precuneus and the prefrontal cortex, anterior cingulate gyrus, and other regions (60). In patients with subclinical depression, the amplitude of low-frequency fluctuation (ALFF) in the right precuneus was significantly increased compared with healthy controls (61). The increased ALFF was also found in the bilateral supramarginal gyrus in a partially-remitted depression group compared with a healthy control group (62). In addition, the ALFF in the right supramarginal gyrus was negatively correlated with the HAMD scores. The inferior parietal lobule, a major network hub of the human brain, is involved in multiple brain networks (e.g., the frontoparietal control network,

default mode network) related to emotional processing and cognitive functions (63). The resting-state functional connectivity was found to be abnormal at the inferior parietal lobule in the late-life depressive patients (64). A previous study showed that patients with depression had significantly impaired parietal lobe function, which may be associated with cognition dysfunction in depressive patients (65). The decreased magnetic susceptibility values in the MCC and PCC and parietal areas suggest the involvement of these regions in the progression of depression.

Altered susceptibility in the subcortical areas as depression progresses

The habenula is a nucleus closely related to depression. Functional MRI studies have revealed that the activity of the habenula is correlated with depressive symptoms (66). Preclinical research has also found that hyperactivity of the lateral habenula is associated with depression, and local bilateral infusion of ketamine into the lateral habenula can elicit rapid antidepressant effects (67,68). Electrical stimulation at a certain frequency targeting the lateral habenula may modulate the degree of depression (69). Iron accumulation in the habenula during the progression of depression over 1 year may be related to the abnormal activity of the habenula neurons involved in depression.

The brainstem contains nuclei of cells synthesizing multiple neurotransmitters modulating depression, such as dopamine, serotonin, and norepinephrine (70). Aberrant structure and function of the brainstem have been found in MDD patients (71,72). Our observation of the increase in susceptibility at the brainstem may be associated with alterations in brainstem cells as depression progresses in patients treated with antidepressants.

A changed QSM value was also found in the cerebellum in our late-life depressive patients. The cerebellum is an area of the hindbrain, and it receives information from the spinal cord, brainstem, and cerebral cortex. Such complex incoming information indicates that the cerebellum is involved in movement, cognitive, and emotional processes. Pieces of evidence from the studies of patients with cerebellar diseases also suggest a possible role of the cerebellum in motor, cognition, and mood (73,74). Patients diagnosed with MDD have shown structural and functional abnormalities in the cerebellum. A high-resolution, structural MRI study showed that MDD is characterized by abnormal volume in non-motor cerebellar regions, and the bilateral cerebellar volume changes may be reflective of

successful anti-depression treatment (75). Previous studies have found that MDD patients have a significantly smaller vermis, a narrow central part of the cerebellum, compared with healthy controls (76). Anatomical findings using MRI have also shown that the cerebellum of MDD patients is smaller than that of healthy controls (77). Furthermore, depressed patients on antidepressant medication have shown increased blood flow in the vermis and increased cerebellar activity (78). Thus, the altered iron deposition in the cerebellum may contribute to the change in the volume and activity of the cerebellum, which may be involved in the progression of depression.

Disrupted cerebellar-cortical connections are also involved in MDD. Ma and colleagues found an abnormal connection between the cerebellum and ACC in medication-naive depressive patients (79). An altered cerebellar-frontal lobe connection has also been reported in patients with geriatric depression (80). Our results of changed magnetic susceptibility values in the mPFC and the dACC, together with the cerebellum, may be related to the disrupted connection between these brain regions.

The iron deposition in the left dorsal striatum (caudate and putamen) was found to be reduced compared with the baseline measurement. Structural abnormalities in the caudate nucleus are frequently found in depression (81). A structural MRI study showed that depressed patients had significantly lower caudate volumes, with the left caudate volume reductions greater than the right, and the volume reductions were correlated with depression severity (82). The susceptibility value was higher in MDD patients than in healthy controls (26). The present study showed that lower left caudate iron deposition may be associated with the progression of depression and antidepressant effects.

Altered susceptibility in white-matter structures

Magnetic susceptibility values can be a quantification measurement of iron and myelin in the white matter structures (83,84). Aside from the gray matter, aberrant white matter structures were also found in MDD patients. A widespread white matter abnormality, including in the corona radiata, has been observed in adult MDD patients, as revealed by a diffusion tensor imaging study (85). The iron content was highly associated with the integrity of white matter structures (86). Our observation that a reduction in depressive symptoms was associated with a decrease in magnetic susceptibility values in the anterior corona radiata suggests that remyelination may occur in white matter

structures related to the alleviation of depressive symptoms in patients on antidepressants.

Limitations

This study had several limitations. First, the study included a relatively small sample size. Studies with larger sample sizes are needed in the future to increase the statistical power and confirm our findings. Second, there was a lack of examination of the QSM alterations in a healthy control group, and thus we could not rule out the possibility that our findings on QSM alterations might result from the normal aging process. In our study, the interval between the 2 scans was approximately 1 year (15 ± 2.1 months), a period of time during which iron content changes could be regarded as minor and part of normal aging (87). Therefore, the iron deposition changes observed in late-life depression in our study might be induced by depression progression. In our results, only the increased magnetic susceptibility value in the left lingula was associated with age, so future studies with a matched control group are still needed. Third, there may be some error in the result regarding the increased QSM value in the habenula. The habenula is a small nucleus, and magnetic susceptibility was heterogeneous within the habenula and across the participants (88,89). The low myelin density may have been the source of elevation of the magnetic susceptibility values, and the veins of the thalamus may have also influenced the analysis of the magnetic susceptibility values in the habenula. Fourth, an observation of a group taking placebo medication could help to reveal the specific influence of antidepressant drugs, and this is recommended for future studies.

Conclusions

Our study primarily identified the brain areas where iron deposition changes as depression progresses in late-life depressive patients. The CMS, occipital areas, habenula, brainstem, and cerebellum showed increasing magnetic susceptibility during the progression of depression in patients on antidepressants. Additionally, the dmPFC, MCC and PCC, parietal and occipital areas, left dorsal striatum, and thalamus showed decreased magnetic susceptibility. Notably, the alterations in the mPFC, dACC, and the nearby white matter area (anterior corona radiata) negatively correlated with alterations in depression scores. Our results strengthen the understanding of the progression of brain iron deposition in late-life depression in patients

on antidepressant medication and highlight the close relationship between magnetic susceptibility in the medial frontal areas and depression.

Acknowledgments

The authors thank all the patients who served as the research participants.

Funding: This work was supported by the National Natural Science Foundation of China (Nos. 61901256 and 91949120 to HW, No. 82101547 to CZ); the Science and Technology Commission of Shanghai Municipality (No. 20DZ2220400 to HW); Shanghai Jiao Tong University (SJTU) Trans-med Awards Research (No. WF540162605/001 to HW, No. WF540162605 to BS); the Innovative Research Team of High-level Local Universities in Shanghai (to NH); and Shanghai Sailing Program (No. 20YF1426500 to CZ).

Footnote

Reporting Checklist: The authors have completed the STROBE reporting checklist. Available at <https://qims.amegroups.com/article/view/10.21037/qims-21-1137/rc>

Conflicts of Interest: All authors have completed the ICMJE uniform disclosure form (available at <https://qims.amegroups.com/article/view/10.21037/qims-21-1137/coif>). HW reports support from the National Natural Science Foundation of China (Nos. 61901256 and 91949120), Science and Technology Commission of Shanghai Municipality (No. 20DZ2220400), and SJTU (Shanghai Jiao Tong University) Trans-med Awards Research (No. WF540162605/001). NH reports support from the Innovative Research Team of High-level Local Universities in Shanghai. BS reports support from SJTU (Shanghai Jiao Tong University) Trans-med Awards Research (No. WF540162605). CZ reports support from the National Natural Science Foundation of China (No. 82101547) and the Shanghai Sailing Program (No. 20YF1426500). The other authors have no conflicts of interest to declare.

Ethical Statement: The authors are accountable for all aspects of the work in ensuring that questions related to the accuracy or integrity of any part of the work are appropriately investigated and resolved. The study was conducted in accordance with the Declaration of Helsinki (as revised in 2013). The study was approved by the Ethics Committee of Shanghai Pudong New Area Mental Health

Center (No. PDJWLL2014001). All participants were informed of the detailed experimental procedures and signed informed consent forms.

Open Access Statement: This is an Open Access article distributed in accordance with the Creative Commons Attribution-NonCommercial-NoDerivs 4.0 International License (CC BY-NC-ND 4.0), which permits the non-commercial replication and distribution of the article with the strict proviso that no changes or edits are made and the original work is properly cited (including links to both the formal publication through the relevant DOI and the license). See: <https://creativecommons.org/licenses/by-nc-nd/4.0/>.

References

1. Malhi GS, Mann JJ. Depression. *Lancet* 2018;392:2299-312.
2. Tedeschini E, Levkovitz Y, Iovieno N, Ameral VE, Nelson JC, Papakostas GI. Efficacy of antidepressants for late-life depression: a meta-analysis and meta-regression of placebo-controlled randomized trials. *J Clin Psychiatry* 2011;72:1660-8.
3. Nomikos GG, Tomori D, Zhong W, Affinito J, Palo W. Efficacy, safety, and tolerability of vortioxetine for the treatment of major depressive disorder in patients aged 55 years or older. *CNS Spectr* 2017;22:348-62.
4. Riddle M, Potter GG, McQuoid DR, Steffens DC, Beyer JL, Taylor WD. Longitudinal Cognitive Outcomes of Clinical Phenotypes of Late-Life Depression. *Am J Geriatr Psychiatry* 2017;25:1123-34.
5. Maeshima H, Baba H, Nakano Y, Satomura E, Namekawa Y, Takebayashi N, Nomoto H, Suzuki T, Mimura M, Arai H. Time course for memory dysfunction in early-life and late-life major depression: a longitudinal study from the Juntendo University Mood Disorder Project. *J Affect Disord* 2013;151:66-70.
6. Liao W, Zhang X, Shu H, Wang Z, Liu D, Zhang Z. The characteristic of cognitive dysfunction in remitted late life depression and amnesic mild cognitive impairment. *Psychiatry Res* 2017;251:168-75.
7. Dybedal GS, Tanum L, Sundet K, Gaarden TL, Bjølseth TM. Neuropsychological functioning in late-life depression. *Front Psychol* 2013;4:381.
8. Potter GG, Madden DJ, Costello MC, Steffens DC. Reduced comparison speed during visual search in late life depression. *J Clin Exp Neuropsychol* 2013;35:1060-70.
9. Rajtar-Zembaty A, Sałakowski A, Rajtar-Zembaty J, Starowicz-Filip A. Executive dysfunction in late-life depression. *Psychiatr Pol* 2017;51:705-18.
10. Kühn S, Gallinat J. Resting-state brain activity in schizophrenia and major depression: a quantitative meta-analysis. *Schizophr Bull* 2013;39:358-65.
11. Hamilton JP, Etkin A, Furman DJ, Lemus MG, Johnson RF, Gotlib IH. Functional neuroimaging of major depressive disorder: a meta-analysis and new integration of base line activation and neural response data. *Am J Psychiatry* 2012;169:693-703.
12. Rodríguez-Cano E, Sarró S, Monté GC, Maristany T, Salvador R, McKenna PJ, Pomarol-Clotet E. Evidence for structural and functional abnormality in the subgenual anterior cingulate cortex in major depressive disorder. *Psychol Med* 2014;44:3263-73.
13. Miller CH, Hamilton JP, Sacchet MD, Gotlib IH. Meta-analysis of Functional Neuroimaging of Major Depressive Disorder in Youth. *JAMA Psychiatry* 2015;72:1045-53.
14. Young KD, Misaki M, Harmer CJ, Victor T, Zotev V, Phillips R, Siegle GJ, Drevets WC, Bodurka J. Real-Time Functional Magnetic Resonance Imaging Amygdala Neurofeedback Changes Positive Information Processing in Major Depressive Disorder. *Biol Psychiatry* 2017;82:578-86.
15. Zeng LL, Shen H, Liu L, Hu D. Unsupervised classification of major depression using functional connectivity MRI. *Hum Brain Mapp* 2014;35:1630-41.
16. Arnone D, McKie S, Elliott R, Juhasz G, Thomas EJ, Downey D, Williams S, Deakin JF, Anderson IM. State-dependent changes in hippocampal grey matter in depression. *Mol Psychiatry* 2013;18:1265-72.
17. Piñero DJ, Connor JR. Iron in the Brain: An Important Contributor in Normal and Diseased States. *The Neuroscientist* 2000;6:435-53.
18. Rouault TA. Iron metabolism in the CNS: implications for neurodegenerative diseases. *Nat Rev Neurosci* 2013;14:551-64.
19. Kim S, Lee Y, Jeon CY, Kim K, Jeon Y, Jin YB, Oh S, Lee C. Quantitative magnetic susceptibility assessed by 7T magnetic resonance imaging in Alzheimer's disease caused by streptozotocin administration. *Quant Imaging Med Surg* 2020;10:789-97.
20. Chen J, Cai T, Li Y, Chi J, Rong S, He C, Li X, Zhang P, Wang L, Zhang Y. Different iron deposition patterns in Parkinson's disease subtypes: a quantitative susceptibility mapping study. *Quant Imaging Med Surg* 2020;10:2168-76.
21. Ward RJ, Zucca FA, Duyn JH, Crichton RR, Zecca L. The role of iron in brain ageing and neurodegenerative disorders. *Lancet Neurol* 2014;13:1045-60.

22. Kim J, Wessling-Resnick M. Iron and mechanisms of emotional behavior. *J Nutr Biochem* 2014;25:1101-7.
23. Zhu L, Han B, Wang L, Chang Y, Ren W, Gu Y, Yan M, Wu C, Zhang XY, He J. The association between serum ferritin levels and post-stroke depression. *J Affect Disord* 2016;190:98-102.
24. Yi S, Nanri A, Poudel-Tandukar K, Nonaka D, Matsushita Y, Hori A, Mizoue T. Association between serum ferritin concentrations and depressive symptoms in Japanese municipal employees. *Psychiatry Res* 2011;189:368-72.
25. Richardson AC, Heath AL, Haszard JJ, Polak MA, Houghton LA, Conner TS. Higher Body Iron Is Associated with Greater Depression Symptoms among Young Adult Men but not Women: Observational Data from the Daily Life Study. *Nutrients* 2015;7:6055-72.
26. Yao S, Zhong Y, Xu Y, Qin J, Zhang N, Zhu X, Li Y. Quantitative Susceptibility Mapping Reveals an Association between Brain Iron Load and Depression Severity. *Front Hum Neurosci* 2017;11:442.
27. Zhang W, Zhou Y, Li Q, Xu J, Yan S, Cai J, Jiaerken Y, Lou M. Brain Iron Deposits in Thalamus Is an Independent Factor for Depressive Symptoms Based on Quantitative Susceptibility Mapping in an Older Adults Community Population. *Front Psychiatry* 2019;10:734.
28. Chen Q, Chen Y, Zhang Y, Wang F, Yu H, Zhang C, Jiang Z, Luo W. Iron deposition in Parkinson's disease by quantitative susceptibility mapping. *BMC Neurosci* 2019;20:23.
29. Du L, Zhao Z, Cui A, Zhu Y, Zhang L, Liu J, Shi S, Fu C, Han X, Gao W, Song T, Xie L, Wang L, Sun S, Guo R, Ma G. Increased Iron Deposition on Brain Quantitative Susceptibility Mapping Correlates with Decreased Cognitive Function in Alzheimer's Disease. *ACS Chem Neurosci* 2018;9:1849-57.
30. WHO. International Statistical Classification of Diseases and Related Health Problems, 10th Revision. Geneva: World Health Organization, 2010.
31. Hamilton M. A rating scale for depression. *J Neurol Neurosurg Psychiatry* 1960;23:56-62.
32. Hamilton M. The assessment of anxiety states by rating. *Br J Med Psychol* 1959;32:50-5.
33. Nasreddine ZS, Phillips NA, Bédirian V, Charbonneau S, Whitehead V, Collin I, Cummings JL, Chertkow H. The Montreal Cognitive Assessment, MoCA: a brief screening tool for mild cognitive impairment. *J Am Geriatr Soc* 2005;53:695-9.
34. Folstein MF, Folstein SE, McHugh PR. "Mini-mental state". A practical method for grading the cognitive state of patients for the clinician. *J Psychiatr Res* 1975;12:189-98.
35. Wei H, Dibb R, Zhou Y, Sun Y, Xu J, Wang N, Liu C. Streaking artifact reduction for quantitative susceptibility mapping of sources with large dynamic range. *NMR Biomed* 2015;28:1294-303.
36. Wei H, Zhang Y, Gibbs E, Chen NK, Wang N, Liu C. Joint 2D and 3D phase processing for quantitative susceptibility mapping: application to 2D echo-planar imaging. *NMR Biomed* 2017;30:e3501.
37. Smith SM. Fast robust automated brain extraction. *Hum Brain Mapp* 2002;17:143-55.
38. Schofield MA, Zhu Y. Fast phase unwrapping algorithm for interferometric applications. *Opt Lett* 2003;28:1194-6.
39. Wu B, Li W, Guidon A, Liu C. Whole brain susceptibility mapping using compressed sensing. *Magn Reson Med* 2012;67:137-47.
40. Tustison NJ, Avants BB, Cook PA, Zheng Y, Egan A, Yushkevich PA, Gee JC. N4ITK: improved N3 bias correction. *IEEE Trans Med Imaging* 2010;29:1310-20.
41. Avants B, Gee JC. Geodesic estimation for large deformation anatomical shape averaging and interpolation. *Neuroimage* 2004;23 Suppl 1:S139-50.
42. Avants BB, Yushkevich P, Pluta J, Minkoff D, Korczykowski M, Detre J, Gee JC. The optimal template effect in hippocampus studies of diseased populations. *Neuroimage* 2010;49:2457-66.
43. Avants BB, Epstein CL, Grossman M, Gee JC. Symmetric diffeomorphic image registration with cross-correlation: evaluating automated labeling of elderly and neurodegenerative brain. *Med Image Anal* 2008;12:26-41.
44. Winkler AM, Ridgway GR, Webster MA, Smith SM, Nichols TE. Permutation inference for the general linear model. *Neuroimage* 2014;92:381-97.
45. Lemogne C, Delaveau P, Freton M, Guionnet S, Fossati P. Medial prefrontal cortex and the self in major depression. *J Affect Disord* 2012;136:e1-11.
46. Drevets WC, Price JL, Furey ML. Brain structural and functional abnormalities in mood disorders: implications for neurocircuitry models of depression. *Brain Struct Funct* 2008;213:93-118.
47. Hare BD, Duman RS. Prefrontal cortex circuits in depression and anxiety: contribution of discrete neuronal populations and target regions. *Mol Psychiatry* 2020;25:2742-58.
48. Dubin MJ, Liston C, Avissar MA, Ilieva I, Gunning FM. Network-Guided Transcranial Magnetic Stimulation for Depression. *Curr Behav Neurosci Rep* 2017;4:70-7.

49. Singh A, Kar SK. How Electroconvulsive Therapy Works?: Understanding the Neurobiological Mechanisms. *Clin Psychopharmacol Neurosci* 2017;15:210-21.
50. Mayberg HS, Lozano AM, Voon V, McNeely HE, Seminowicz D, Hamani C, Schwalb JM, Kennedy SH. Deep brain stimulation for treatment-resistant depression. *Neuron* 2005;45:651-60.
51. Salami A, Avelar-Pereira B, Garzón B, Sitnikov R, Kalpouzos G. Functional coherence of striatal resting-state networks is modulated by striatal iron content. *Neuroimage* 2018;183:495-503.
52. Lai CH. Promising Neuroimaging Biomarkers in Depression. *Psychiatry Investig* 2019;16:662-70.
53. Lai CH, Wu YT. The alterations in regional homogeneity of parieto-cingulate and temporo-cerebellum regions of first-episode medication-naïve depression patients. *Brain Imaging Behav* 2016;10:187-94.
54. Peng DH, Jiang KD, Fang YR, Xu YF, Shen T, Long XY, Liu J, Zang YF. Decreased regional homogeneity in major depression as revealed by resting-state functional magnetic resonance imaging. *Chin Med J (Engl)* 2011;124:369-73.
55. Li J, Xu C, Cao X, Gao Q, Wang Y, Wang Y, Peng J, Zhang K. Abnormal activation of the occipital lobes during emotion picture processing in major depressive disorder patients. *Neural Regen Res* 2013;8:1693-701.
56. Salvador GA, Uranga RM, Giusto NM. Iron and mechanisms of neurotoxicity. *Int J Alzheimers Dis* 2010;2011:720658.
57. Yang R, Gao C, Wu X, Yang J, Li S, Cheng H. Decreased functional connectivity to posterior cingulate cortex in major depressive disorder. *Psychiatry Res Neuroimaging* 2016;255:15-23.
58. Cheng W, Rolls ET, Qiu J, Xie X, Wei D, Huang CC, Yang AC, Tsai SJ, Li Q, Meng J, Lin CP, Xie P, Feng J. Increased functional connectivity of the posterior cingulate cortex with the lateral orbitofrontal cortex in depression. *Transl Psychiatry* 2018;8:90.
59. Zhou M, Hu X, Lu L, Zhang L, Chen L, Gong Q, Huang X. Intrinsic cerebral activity at resting state in adults with major depressive disorder: A meta-analysis. *Prog Neuropsychopharmacol Biol Psychiatry* 2017;75:157-64.
60. Cheng W, Rolls ET, Qiu J, Yang D, Ruan H, Wei D, Zhao L, Meng J, Xie P, Feng J. Functional Connectivity of the Precuneus in Unmedicated Patients With Depression. *Biol Psychiatry Cogn Neurosci Neuroimaging* 2018;3:1040-9.
61. Zhang B, Qi S, Liu S, Liu X, Wei X, Ming D. Altered spontaneous neural activity in the precuneus, middle and superior frontal gyri, and hippocampus in college students with subclinical depression. *BMC Psychiatry* 2021;21:280.
62. Liu CH, Ma X, Song LP, Tang LR, Jing B, Zhang Y, Li F, Zhou Z, Fan J, Wang CY. Alteration of spontaneous neuronal activity within the salience network in partially remitted depression. *Brain Res* 2015;1599:93-102.
63. Igelström KM, Graziano MSA. The inferior parietal lobule and temporoparietal junction: A network perspective. *Neuropsychologia* 2017;105:70-83.
64. Li J, Gong H, Xu H, Ding Q, He N, Huang Y, Jin Y, Zhang C, Voon V, Sun B, Yan F, Zhan S. Abnormal Voxel-Wise Degree Centrality in Patients With Late-Life Depression: A Resting-State Functional Magnetic Resonance Imaging Study. *Front Psychiatry* 2020;10:1024.
65. Freedman M. Frontal and parietal lobe dysfunction in depression: delayed alternation and tactile learning deficits. *Neuropsychologia* 1994;32:1015-25.
66. Lawson RP, Nord CL, Seymour B, Thomas DL, Dayan P, Pilling S, Roiser JP. Disrupted habenula function in major depression. *Mol Psychiatry* 2017;22:202-8.
67. Li B, Piriz J, Mirrione M, Chung C, Proulx CD, Schulz D, Henn F, Malinow R. Synaptic potentiation onto habenula neurons in the learned helplessness model of depression. *Nature* 2011;470:535-9.
68. Yang Y, Cui Y, Sang K, Dong Y, Ni Z, Ma S, Hu H. Ketamine blocks bursting in the lateral habenula to rapidly relieve depression. *Nature* 2018;554:317-22.
69. Sartorius A, Kiening KL, Kirsch P, von Gall CC, Haberkorn U, Unterberg AW, Henn FA, Meyer-Lindenberg A. Remission of major depression under deep brain stimulation of the lateral habenula in a therapy-refractory patient. *Biol Psychiatry* 2010;67:e9-11.
70. Azizi SA. Monoamines: Dopamine, Norepinephrine, and Serotonin, Beyond Modulation, "Switches" That Alter the State of Target Networks. *Neuroscientist* 2022;28:121-43.
71. Supprian T, Reiche W, Schmitz B, Grunwald I, Backens M, Hofmann E, Georg T, Falkai P, Reith W. MRI of the brainstem in patients with major depression, bipolar affective disorder and normal controls. *Psychiatry Res* 2004;131:269-76.
72. Smith R, Allen JJ, Thayer JF, Lane RD. Altered functional connectivity between medial prefrontal cortex and the inferior brainstem in major depression during appraisal of subjective emotional responses: A preliminary study. *Biol Psychol* 2015;108:13-24.
73. Schmahmann JD. Disorders of the cerebellum: ataxia, dysmetria of thought, and the cerebellar cognitive affective syndrome. *J Neuropsychiatry Clin Neurosci* 2004;16:367-78.

74. Schutter DJ, van Honk J. The cerebellum in emotion regulation: a repetitive transcranial magnetic stimulation study. *Cerebellum* 2009;8:28-34.
75. Depping MS, Wolf ND, Vasic N, Sambataro F, Hirjak D, Thomann PA, Wolf RC. Abnormal cerebellar volume in acute and remitted major depression. *Prog Neuropsychopharmacol Biol Psychiatry* 2016;71:97-102.
76. Yucel K, Nazarov A, Taylor VH, Macdonald K, Hall GB, Macqueen GM. Cerebellar vermis volume in major depressive disorder. *Brain Struct Funct* 2013;218:851-8.
77. Brambilla P, Barale F, Caverzasi E, Soares JC. Anatomical MRI findings in mood and anxiety disorders. *Epidemiol Psychiatr Soc* 2002;11:88-99.
78. Phillips JR, Hewedi DH, Eissa AM, Moustafa AA. The cerebellum and psychiatric disorders. *Front Public Health* 2015;3:66.
79. Ma Q, Zeng LL, Shen H, Liu L, Hu D. Altered cerebellar-cerebral resting-state functional connectivity reliably identifies major depressive disorder. *Brain Res* 2013;1495:86-94.
80. Alalade E, Denny K, Potter G, Steffens D, Wang L. Altered cerebellar-cerebral functional connectivity in geriatric depression. *PLoS One* 2011;6:e20035.
81. Krishnan KR, McDonald WM, Escalona PR, Doraiswamy PM, Na C, Husain MM, Figiel GS, Boyko OB, Ellinwood EH, Nemeroff CB. Magnetic resonance imaging of the caudate nuclei in depression. Preliminary observations. *Arch Gen Psychiatry* 1992;49:553-7.
82. Butters MA, Aizenstein HJ, Hayashi KM, Meltzer CC, Seaman J, Reynolds CF 3rd, Toga AW, Thompson PM, Becker JT; IMAGE Research Group. Three-dimensional surface mapping of the caudate nucleus in late-life depression. *Am J Geriatr Psychiatry* 2009;17:4-12.
83. Wisnieff C, Ramanan S, Olesik J, Gauthier S, Wang Y, Pitt D. Quantitative susceptibility mapping (QSM) of white matter multiple sclerosis lesions: Interpreting positive susceptibility and the presence of iron. *Magn Reson Med* 2015;74:564-70.
84. Ravanfar P, Loi SM, Syeda WT, Van Rheenen TE, Bush AI, Desmond P, Copley VL, Lane DJR, Opazo CM, Moffat BA, Velakoulis D, Pantelis C. Systematic Review: Quantitative Susceptibility Mapping (QSM) of Brain Iron Profile in Neurodegenerative Diseases. *Front Neurosci* 2021;15:618435.
85. van Velzen LS, Kelly S, Isaev D, Aleman A, Aftanas LI, Bauer J, et al. White matter disturbances in major depressive disorder: a coordinated analysis across 20 international cohorts in the ENIGMA MDD working group. *Mol Psychiatry* 2020;25:1511-25.
86. Khattar N, Triebswetter C, Kiely M, Ferrucci L, Resnick SM, Spencer RG, Bouhrara M. Investigation of the association between cerebral iron content and myelin content in normative aging using quantitative magnetic resonance neuroimaging. *Neuroimage* 2021;239:118267.
87. Gong NJ, Wong CS, Hui ES, Chan CC, Leung LM. Hemisphere, gender and age-related effects on iron deposition in deep gray matter revealed by quantitative susceptibility mapping. *NMR Biomed* 2015;28:1267-74.
88. Yoo S, Kim JW, Schenck JF, Lee SK. Magnetic susceptibility imaging of human habenula at 3 T. *Sci Rep* 2020;10:19357.
89. He N, Sethi SK, Zhang C, Li Y, Chen Y, Sun B, Yan F, Haacke EM. Visualizing the lateral habenula using susceptibility weighted imaging and quantitative susceptibility mapping. *Magn Reson Imaging* 2020;65:55-61.

Cite this article as: Wang F, Zhang M, Li Y, Li Y, Gong H, Li J, Zhang Y, Zhang C, Yan F, Sun B, He N, Wei H. Alterations in brain iron deposition with progression of late-life depression measured by magnetic resonance imaging (MRI)-based quantitative susceptibility mapping. *Quant Imaging Med Surg* 2022;12(7):3873-3888. doi: 10.21037/qims-21-1137

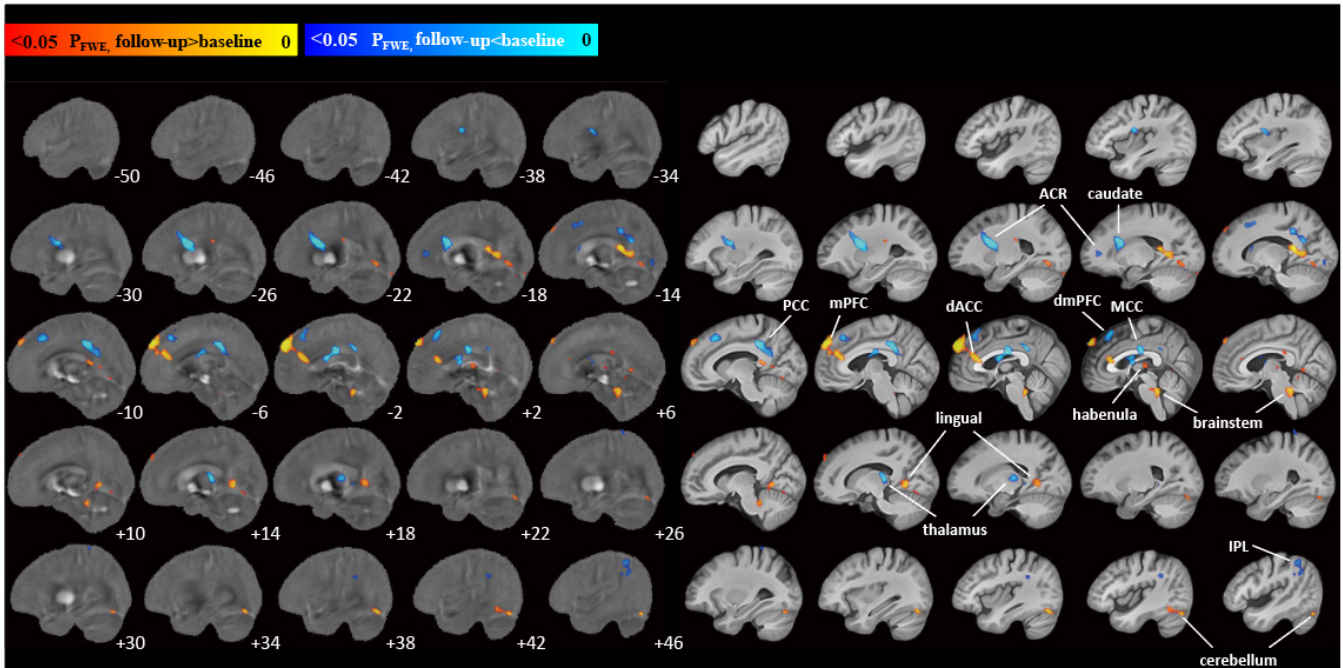


Figure S1 The sagittal projections of the whole-brain susceptibility values change around one year in the patients overlaid on the QSM template and the T1 template in the MNI space by voxel-wise analysis. The red/yellow clusters represent a higher susceptibility value in the follow-up/the second visit ($P < 0.05$, FWE corrected). The blue/light blue clusters represent a lower susceptibility value in the follow-up/the second visit ($P < 0.05$, FWE corrected). The numbers represent the sagittal coordinates of the slice in millimeters in MNI coordinate space. ($P < 0.05$, FWE corrected). FWE, family-wise error; ACR, anterior corona radiata; PCC, posterior cingulate cortex; mPFC, medial prefrontal cortex; dACC, dorsal anterior cingulate cortex; dmPFC, dorsal medial prefrontal cortex; MCC, middle cingulate cortex; IPL, inferior parietal lobule; QSM, quantitative susceptibility mapping; MNI, Montreal Neurological Institute.

Table S1 Brain areas showed increased QSM value after an approximately one-year duration in the depressive patients ($P < 0.05$, FWE corrected)

Cluster index	Peak MNI coordinates (x mm, y mm, z mm)	Peak intensity	Cluster's voxel number	Anatomical name	Brodmann area
Cluster #1 (mPFC and dACC)	(-3, 58, 35)	0.997	5,548	Cingulum_Ant_sup_L, Cingulum_Ant_sup_R, Frontal_Sup_Medial_L, Frontal_Sup_Medial_R, Frontal_Sup_R, Frontal_Sup_L	BA6, 8, 9, 10, 24, 32
Cluster #2 (middle cingulate)	(6, -31, 26)	0.962	88	Cingulum_Mid_R	BA23
Cluster #3 (left lingual)	(-21, -71, -7)	0.978	664	Lingual_L, Cerebellum_6_L	BA18, 19
Cluster #4 (right lingual)	(13, -57, -1)	0.991	1,345	Cerebellum_4_5_R, Lingual_R, Calcarine_R, Vermis_4_5	BA18, 19, 29, 30
Cluster #5 (right lingual)	(11, -70, -9)	0.960	110	Cerebellum_6_R, Lingual_R	BA18, 19
Cluster #6 (white matter and left calcarine)	(-15, -42, 14)	0.996	2,109	Corpus_Callosum_Splenium_L, Calcarine_L, Cingulum_Post_L, Precuneus_L	BA18, 29, 30
Cluster #7 (habenula)	(3, -21, 8)	0.973	247	Thalamus_L, Thalamus_R	-
Cluster #8 (brainstem and cerebellum)	(1, -38, -27)	0.992	1,575	Cerebellum_3_R, Vermis_1_2	-
Cluster #9 (cerebellum and fusiform)	(38, -72, -18)	0.991	1,461	Cerebellum_Crus1_R, Fusiform_R, Cerebellum_6_R, Temporal_Inf_R	BA18, 19, 37
Cluster #10 (cerebellum)	(-19, -81, -25)	0.955	13	Cerebellum_Crus1_L	-
Cluster #11 (cerebellum)	(-21, -92, -22)	0.970	75	Cerebellum_Crus1_L	-
Cluster #12 (white matter)	(-25, -28, 24)	0.978	155	Posterior_Corona_Radiata_L	-

The anatomical name indicates the names of the Automated Anatomical Labeling (3rd version) or ICBM DTI-81 atlases. QSM, quantitative susceptibility mapping; FWE, family-wise error; MNI, Montreal Neurological Institute; mPFC, medial prefrontal cortex; dACC, dorsal anterior cingulate cortex.

Table S2 Brain areas showed decreased QSM value after an approximately one-year duration in the depressive patients ($P < 0.05$, FWE corrected)

Cluster index	Peak MNI coordinates (x mm, y mm, z mm)	Peak intensity	Cluster's voxel number	Anatomical name	Brodmann area
Cluster #1 (dmPFC)	(2, 29, 52)	0.987	2,566	Frontal_Sup_Medial_R, Frontal_Sup_Medial_L, Supp_Motor_Area_L, Frontal_Sup_L	BA6, 8, 32
Cluster #2 (MCC)	(-1, -14, 31)	0.997	2,389	Cingulum_Mid_L, Cingulum_Mid_R	BA23, 24
Cluster #3 (MCC and PCC)	(-6, -38, 37)	0.999	3,117	Cingulum_Mid_L, Cingulum_Mid_R, Cingulum_Post_L, Cingulum_Post_R	BA31
Cluster #4 (right postcentral)	(28, -43, 72)	0.968	211	Postcentral_R	BA2, 5
Cluster #5 (right inferior parietal)	(47, -46, 51)	0.979	755	Parietal_Inf_R	BA40
Cluster #6 (right precuneus)	(16, -38, 3)	0.962	75	Precuneus_R	BA30
Cluster #7 (right supramarginal)	(42, -41, 32)	0.962	320	SupraMarginal_R	BA40
Cluster #8 (left lingual)	(-14, -85, -7)	0.964	133	Lingual_L	BA17
Cluster #9 (right thalamus)	(14, -26, 10)	0.996	956	Thalamus_R	-
Cluster #10 (left dorsal striatum and white matter)	(-23, 8, 22)	0.9996	5,295	Caudate_L, Putamen_L, Rolandic_Oper_L, Insula_L, Anterior_Corona_Radiata_L	-
Cluster #11 (white matter)	(-18, 44, 6)	0.970	246	Anterior_Corona_Radiata_L	-

The anatomical name indicates the names of the Automated Anatomical Labeling (3rd version) or ICBM DTI-81 atlases. QSM, quantitative susceptibility mapping; FWE, family-wise error; MNI, Montreal Neurological Institute; dmPFC, dorsal medial prefrontal cortex; MCC, middle cingulate cortex; PCC, posterior cingulate cortex.

Table S3 Correlations between the increases in QSM measures and the changes in clinical measurements

Cluster index	Partial Spearman correlation [r (P)]				
	HAMD-17	HAMD-24	HAMA	MMSE	MoCA
Cluster #1 (mPFC and dACC)	-0.613 (0.009)	-0.542 (0.025)	-0.343 (0.178)	-0.166 (0.523)	-0.308 (0.229)
Cluster #2 (middle cingulate)	-0.237 (0.359)	-0.195 (0.454)	-0.161 (0.538)	0.042 (0.874)	-0.105 (0.690)
Cluster #3 (left lingual)	-0.153 (0.557)	-0.107 (0.682)	0.097 (0.710)	-0.410 (0.102)	0.132 (0.613)
Cluster #4 (right lingual)	-0.109 (0.678)	-0.113 (0.666)	0.111 (0.671)	-0.408 (0.104)	0.000 (0.999)
Cluster #5 (right lingual)	-0.166 (0.525)	-0.230 (0.374)	0.044 (0.867)	-0.016 (0.951)	-0.100 (0.703)
Cluster #6 (white matter and left calcarine)	-0.287 (0.264)	-0.181 (0.490)	-0.227 (0.380)	-0.472 (0.055)	-0.046 (0.860)
Cluster #7 (habenula)	-0.024 (0.927)	-0.029 (0.912)	-0.236 (0.362)	-0.588 (0.013)	-0.008 (0.974)
Cluster #8 (brainstem and cerebellum)	-0.153 (0.559)	-0.118 (0.652)	-0.141 (0.589)	-0.230 (0.375)	0.119 (0.648)
Cluster #9 (cerebellum and fusiform)	-0.221 (0.395)	-0.166 (0.525)	0.019 (0.943)	-0.038 (0.885)	-0.220 (0.395)
Cluster #10 (cerebellum)	-0.154 (0.555)	0.018 (0.946)	-0.316 (0.217)	-0.500 (0.041)	0.423 (0.091)
Cluster #11 (cerebellum)	0.035 (0.893)	0.143 (0.584)	0.117 (0.655)	0.164 (0.528)	0.322 (0.208)
Cluster #12 (white matter)	-0.358 (0.158)	-0.193 (0.459)	-0.282 (0.273)	-0.288 (0.266)	-0.062 (0.814)

The r and P values are from partial Spearman correlation analyses adjusting for age, gender, and the interval between two visits. QSM, quantitative susceptibility mapping; HAMD, Hamilton Depression Scales; HAMA, Hamilton Anxiety Scale; MMSE, Mini-Mental State Examination; MoCA, Montreal Cognitive Assessment; mPFC, medial prefrontal cortex; dACC, dorsal anterior cingulate cortex.

Table S4 Correlations between the decreases in QSM measures and the changes in clinical measurements

Cluster index	Partial Spearman correlation [r (P)]				
	HAMD-17	HAMD-24	HAMA	MMSE	MoCA
Cluster #1 (dmPFC)	-0.014 (0.958)	-0.035 (0.666)	0.056 (0.832)	0.080 (0.761)	0.225 (0.385)
Cluster #2 (MCC)	-0.190 (0.465)	-0.093 (0.722)	-0.155 (0.554)	-0.139 (0.594)	0.046 (0.862)
Cluster #3 (MCC and PCC)	-0.276 (0.283)	-0.169 (0.516)	-0.004 (0.987)	-0.189 (0.467)	-0.007 (0.979)
Cluster #4 (right postcentral)	-0.375 (0.138)	-0.391 (0.121)	-0.406 (0.106)	-0.188 (0.469)	-0.347 (0.172)
Cluster #5 (right inferior parietal)	-0.355 (0.162)	-0.278 (0.280)	-0.180 (0.489)	0.211 (0.416)	-0.182 (0.486)
Cluster #6 (right precuneus)	-0.165 (0.526)	-0.149 (0.568)	-0.162 (0.534)	-0.174 (0.504)	0.129 (0.620)
Cluster #7 (right supramarginal)	-0.225 (0.385)	-0.270 (0.295)	-0.022 (0.933)	-0.352 (0.166)	-0.029 (0.913)
Cluster #8 (left lingual)	0.055 (0.834)	-0.013 (0.960)	0.283 (0.271)	-0.613 (0.009)	0.450 (0.070)
Cluster #9 (right thalamus)	0.064 (0.809)	0.055 (0.833)	0.180 (0.489)	-0.517 (0.033)	0.072 (0.782)
Cluster #10 (left dorsal striatum and white matter)	-0.100 (0.703)	0.041 (0.877)	-0.009 (0.973)	0.066 (0.800)	-0.181 (0.486)
Cluster #11 (white matter)	-0.541 (0.025)	-0.500 (0.041)	-0.120 (0.646)	0.015 (0.953)	0.230 (0.375)

The r and P values are from partial Spearman correlation analyses adjusting for age, gender, and the interval between two visits. QSM, quantitative susceptibility mapping; HAMD, Hamilton Depression Scales; HAMA, Hamilton Anxiety Scale; MMSE, Mini-Mental State Examination; MoCA, Montreal Cognitive Assessment; dmPFC, dorsal medial prefrontal cortex; MCC, middle cingulate cortex; PCC, posterior cingulate cortex.